


## Empowering Control of Antiferromagnets by THz-Induced Spin Coherence

T. G. H. Blank<sup>1,\*</sup>, K. A. Grishunin<sup>1</sup>, B. A. Ivanov<sup>1,2</sup>, E. A. Mashkovich<sup>3</sup>, D. Afanasiev<sup>1</sup>, and A. V. Kimel<sup>1</sup>

<sup>1</sup>*Radboud University, Institute for Molecules and Materials, 6525 AJ Nijmegen, The Netherlands*

<sup>2</sup>*Institute of Magnetism, National Academy of Sciences and Ministry of Education and Science, 03142 Kiev, Ukraine*

<sup>3</sup>*Institute of Physics II, University of Cologne, D-50937 Cologne, Germany*

 (Received 31 March 2023; accepted 27 July 2023; published 29 August 2023)

Finding efficient and ultrafast ways to control antiferromagnets is believed to be instrumental in unlocking their potential for magnetic devices operating at THz frequencies. Still, it is challenged by the absence of net magnetization in the ground state. Here, we show that the magnetization emerging from a state of coherent spin precession in antiferromagnetic iron borate FeBO<sub>3</sub> can be used to enable the nonlinear coupling of light to another, otherwise weakly susceptible, mode of spin precession. This nonlinear mechanism can facilitate conceptually new ways of controlling antiferromagnetism.

DOI: 10.1103/PhysRevLett.131.096701

Thermodynamic theory models a simple antiferromagnet as two ferromagnets with two mutually equal, but oppositely oriented, magnetizations  $\mathbf{M}_1$  and  $\mathbf{M}_2$ . As the net magnetization  $\mathbf{M} = \mathbf{M}_1 + \mathbf{M}_2$  is zero, the spin order is described by the nonzero antiferromagnetic Néel vector  $\mathbf{L} = \mathbf{M}_1 - \mathbf{M}_2$ . However, the Néel vector  $\mathbf{L}$  in thermodynamic equilibrium is notoriously insusceptible to external magnetic fields [1]. Despite the 60-year-long search for thermodynamic field conjugates to the antiferromagnetic order parameter [2], through which it may be altered, efficient mechanisms to control antiferromagnets are still at the focus of fundamental research, hampering further developments of antiferromagnetic spintronics, magnonics, and data storage [1,3,4].

Out of equilibrium, the situation changes dramatically. Absolutely every antiferromagnet can be driven in a non-equilibrium coherent magnonic state with nonzero dynamic net magnetization  $\mathbf{M}(t)$ , by resonantly driving  $\mathbf{L}(t)$  with a THz magnetic field  $\mathbf{h}(t)$  applied perpendicular to the spins [5]. The emerging dynamic net magnetization follows from elementary Lagrangian mechanics, which shows that [6–8]

$$\mathbf{M}(t) = \frac{1}{2\gamma H_{\text{ex}} M_0} \left[ \mathbf{L} \times \frac{d\mathbf{L}}{dt} \right], \quad (1)$$

where  $\gamma$  is the gyromagnetic ratio,  $H_{\text{ex}}$  is the antiferromagnetic exchange field, and  $M_0 \equiv |\mathbf{M}_{1,2}|$ . Once in the coherent magnonic state, the antiferromagnet is characterized by an enhanced susceptibility to magnetic field, as the latter can couple to the dynamic magnetization  $\mathbf{M}(t)$ . Hence, when preparing an antiferromagnet in a coherent magnonic state first with a preparation pulse  $\mathbf{h}_1(t)$  applied perpendicular to the spins, the resulting dynamic magnetization greatly enhances the susceptibility to the magnetic field of a subsequent excitation pulse  $\mathbf{h}_2(t)$  applied along the equilibrium spin direction (see Fig. 1 for an illustration

of this idea). This means that the response of an antiferromagnet to a pair of pulses of magnetic fields,  $\mathbf{h}_1(t)$  and  $\mathbf{h}_2(t)$ , can be much larger than the effects caused by each of the pulses taken alone, and is therefore beyond trivial superposition.

To explore this mechanism for empowering THz control of antiferromagnetism, we employ the principles of two-dimensional (2D) THz spectroscopy [9–14]. This spectroscopic technique was previously applied to study nonlinearities of spin resonances in Ref. [15]. In this technique, two intense THz pump pulses are applied

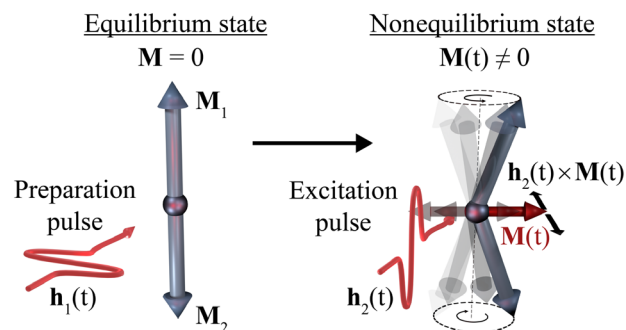


FIG. 1. Enhanced susceptibility of antiferromagnets via a coherent magnonic state. Left: magnetic configuration of a collinear antiferromagnet in equilibrium. The two arrows indicate the magnetizations of the antiferromagnetically coupled sublattices  $\mathbf{M}_1$  and  $\mathbf{M}_2$  with  $\mathbf{M}_1 = -\mathbf{M}_2$  such that the net magnetization is absent  $\mathbf{M} = 0$ . However, by applying a “preparation pulse” with the magnetic field  $\mathbf{h}_1(t)$  perpendicular to the spins, it is possible to generate a coherent magnonic state, inducing a dynamic magnetization  $\mathbf{M}(t)$  as depicted on the right. Right: once in the nonequilibrium state, a second THz “excitation pulse” polarized along the equilibrium spin direction will now be able to exert a nonzero dynamic torque  $\mathbf{h}_2(t) \times \mathbf{M}(t)$ . The susceptibility of the antiferromagnet is thereby enhanced via a coherent magnonic state.

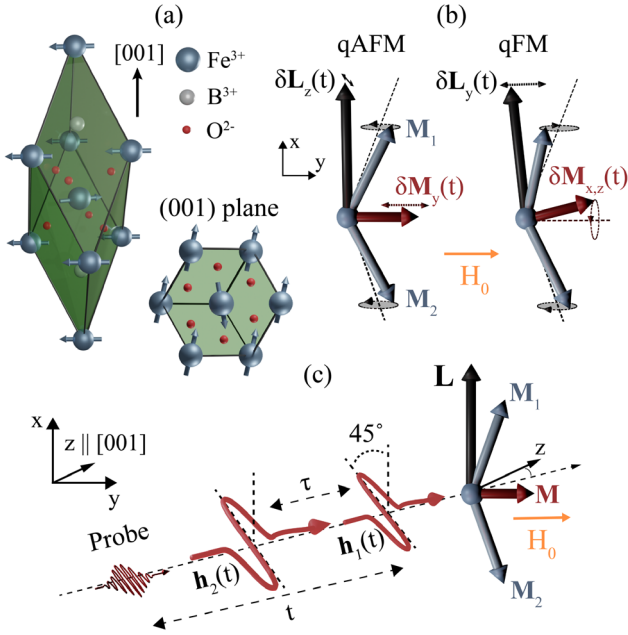


FIG. 2. (a) Primitive unit cell of the FeBO<sub>3</sub> crystal with the Fe<sup>3+</sup> spins indicated by arrows. (b) The two eigenmodes of spin precession of a canted antiferromagnet. (c) A schematic illustration of 2D THz spectroscopy in FeBO<sub>3</sub>. The probe pulse (pulse duration  $\sim 100$  fs, central wavelength 800 nm) electric field was polarized along the  $y$  axis.

successively to the material, mutually separated by an *excitation time* delay  $\tau$ . By measuring the rotation of polarization by magneto-optical effects of an ultrashort near-infrared or visible probe pulse delayed by the *detection time*  $t$ , one can trace magnetization dynamics  $\mathbf{M}(t)$  in the form of probe polarization rotation  $\theta(t)$  induced both by the combined action of the pump pulses  $\theta_{12}(t, \tau)$  and by each of the pump pulses separately— $\theta_1(t, \tau)$  and  $\theta_2(t, \tau)$ . The nonlinear part of spin dynamics that stands beyond the trivial superposition can be readily extracted from the total signal by finding the difference  $\theta_{NL}(t, \tau) = \theta_{12}(t, \tau) - \theta_1(t, \tau) - \theta_2(t, \tau)$ . Note that the polarization rotation may include contributions induced by the THz pulses unrelated to spin dynamics.

Here we apply this technique to FeBO<sub>3</sub>—a prototypical antiferromagnet ideally suitable for time-resolved magneto-optical pump-probe experiments. For temperatures below the Néel point  $T_N \approx 348$  K, the Fe<sup>3+</sup> spins in this material form two equivalent antiferromagnetically coupled macroscopic sublattice magnetizations  $\mathbf{M}_1$  and  $\mathbf{M}_2$  lying in the (001) sample plane [16] [see Fig. 2(a)]. In equilibrium the magnetization vectors are slightly canted at an angle of  $\sim 1^\circ$  because of the Dzyaloshinskii-Moriya interaction [17], resulting in a small net magnetization  $\mathbf{M}$  perpendicular to  $\mathbf{L}$ . The material hosts two nondegenerate mutually orthogonal modes of spin precession, with significantly different frequencies: the quasiantiferromagnetic (qAFM) and quasiferromagnetic (qFM) modes [18] [see Fig. 2(b)]. The qAFM mode essentially results in out-of-plane motion

of the Néel vector and in longitudinal dynamics of the net magnetization  $\mathbf{M}$  ( $f_{AFM} \approx 0.5$  THz at  $T = 78$  K), while the qFM mode ( $f_{FM} \approx 0.03$  THz at  $T = 78$  K) is mainly associated with in-plane dynamics of  $\mathbf{L}$  and results in transverse precessional dynamics of  $\mathbf{M}$  [19]. Most importantly, the material is characterized by strong magneto-optical effects which facilitate sensitive detection of magnetization dynamics  $\mathbf{M}(t)$  with the help of light [16,20–22]. Finally, the choice of FeBO<sub>3</sub> is motivated by recent experiments which showed that an intense single-cycle THz pulse can excite both modes simultaneously [23]. Here, the amplitude of the qAFM mode scaled linearly while that of the qFM scaled quadratically with the THz magnetic field. The linear excitation of the qAFM mode could be explained in terms of a magnetic-dipole interaction or Zeeman torque of the THz magnetic field with spins [24], which is maximal when the THz magnetic field is perpendicular to  $\mathbf{L}$ . The mechanism of the nonlinear excitation of the qFM mode is still unknown.

The experimental geometry is illustrated in Fig. 2(c). The two THz pulses with peak magnetic fields of about 110 mT (see Supplemental Material [25]) were incident on the sample approximately along the [001] crystallographic axis, but at a slight angle ( $\sim 12^\circ$ ) away from this axis because we tilted the sample as in Ref. [23]. The FeBO<sub>3</sub> sample was cooled down to 78 K where the observed dynamics were optimal. A static external magnetic field  $\mu_0 \mathbf{H}_0 \approx 70$  mT was applied predominantly in the (001) easy plane to control the in-plane orientation of  $\mathbf{M}$ . The direction of the aligned magnetization is referred to as the  $y$  axis. The polarization of the THz magnetic fields was set to  $45^\circ$  from the  $y$  axis. By setting this THz polarization, we ensured that the first THz pulse contains a strong THz magnetic field component perpendicular to the spins to excite the qAFM mode [24], while the second pulse has a large component perpendicular to the anticipated emergent dynamic magnetization.

Figure 3 summarizes the results of the 2D time-resolved measurements. In particular, Fig. 3(a) shows the calibrated magnetic response from the combined action of the two THz pulses  $\theta_{12}(t, \tau)$ . It is seen that fast oscillations in time  $t$ , which can be assigned to the qAFM mode, are intertwined with slower oscillations at the frequency typical for the qFM mode  $f_{FM}$ . A striking feature of these data is the periodic dependence of the amplitude of the low-frequency (qFM) mode as a function of the excitation time delay  $\tau$ , which can be seen in the 2D mapping as equidistant white horizontal stripes. According to the color code, the white color corresponds to zero amplitude. This is seen even more directly in Fig. 3(b), which shows a selection of time traces obtained at different  $\tau$ . It is seen that subtle changes in the excitation time delay  $\tau \ll f_{FM}^{-1}$  have a dramatic impact on the amplitude of the mode, practically switching it “on” and “off.” In fact, the toggling of the qFM mode as a function of  $\tau$  has a periodicity  $\Delta\tau$  that can be related to the frequency of

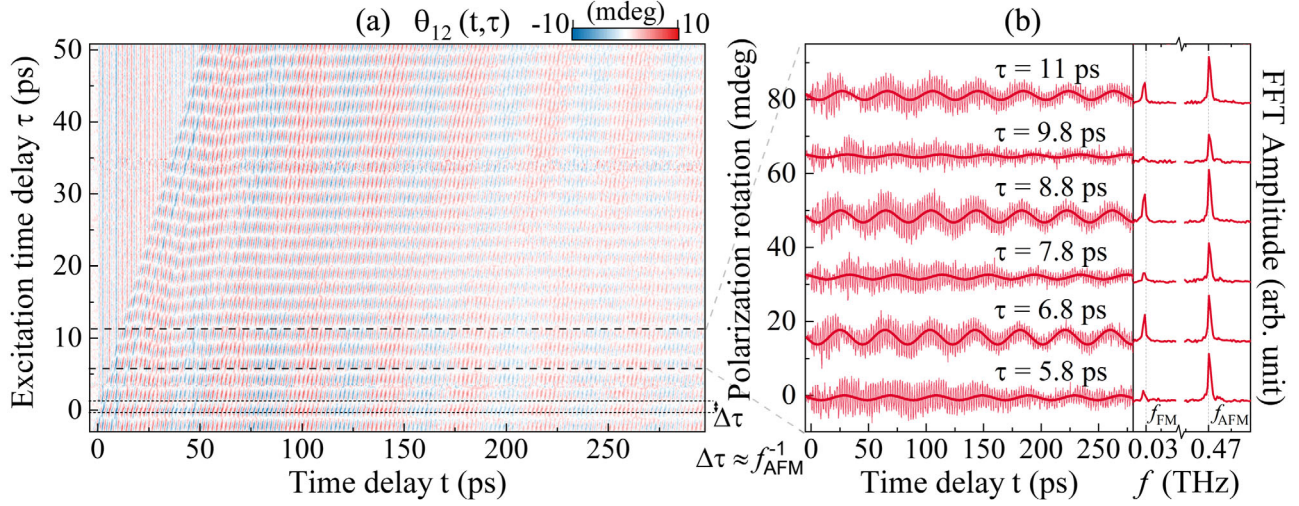


FIG. 3. Time-domain result of 2D THz spectroscopy in FeBO<sub>3</sub>. (a) Double THz pump induced polarization rotation of the probe  $\theta_{12}(t, \tau)$  as a function of the detection time delay  $t$  and the excitation time delay  $\tau$  [see Fig. 2(c)]. The regions where the qFM mode is seen to be quenched are separated by a characteristic time  $\Delta\tau \approx f_{\text{AFM}}^{-1}$ . (b) Cross section of the two-dimensional graph and the associated FFT depicted for several  $\tau$ , emphasizing the toggling of the qFM mode with a repetition rate that can be associated with the qAFM mode.

the qAFM mode  $\Delta\tau \approx f_{\text{AFM}}^{-1}$ . This observation is in line with the anticipated nonlinear mechanism shown in Fig. 1 and can be intuitively linked to the dynamics of the qAFM mode shown in Fig. 2(b): if the first THz pulse excited the qAFM mode with associated dynamic magnetization  $\delta\mathbf{M}_y(t)$ , then depending on the arrival time  $\tau$  of the second THz pulse  $\mathbf{h}_2(t, \tau)$ , the momentary length of the net magnetization  $\mathbf{M} + \delta\mathbf{M}_y(t)$  will be either long or short, oscillating at the frequency  $f_{\text{AFM}}$ . Therefore, the torque exerted by the second THz pulse  $\mathbf{h}_2(t, \tau) \times [\mathbf{M} + \delta\mathbf{M}_y(t)]$ , and hence the excitation of the qFM mode, will be either strong or weak, respectively, modulated at the frequency of the qAFM mode.

The 2D time-resolved data can also be presented in reciprocal space using the two-dimensional fast Fourier transform (2D FFT). Especially the nonlinear data  $\theta_{\text{NL}}(t, \tau)$  are easier to interpret in Fourier space given the low signal-to-noise ratio of the time-resolved data (see Supplemental Material [25]). The conjugate frequencies to the times  $t$  and  $\tau$  are referred to as *detection frequency*  $f_{\text{det}}$  and *excitation frequency*  $f_{\text{ex}}$ , respectively. In the 2D FFT mapping, all linear contributions appear at the diagonal  $f_{\text{det}} = f_{\text{ex}}$ , while second-order nonlinearities generally appear away from the diagonal [9,13,15,33]. Figure 4(a) shows the 2D Fourier amplitude for the nonlinear signal  $\tilde{\theta}_{\text{NL}}(f_{\text{det}}, f_{\text{ex}})$ , which clearly reveals maxima at  $(f_{\text{det}}, f_{\text{ex}}) \approx (\pm f_{\text{FM}}, \pm f_{\text{AFM}})$ .

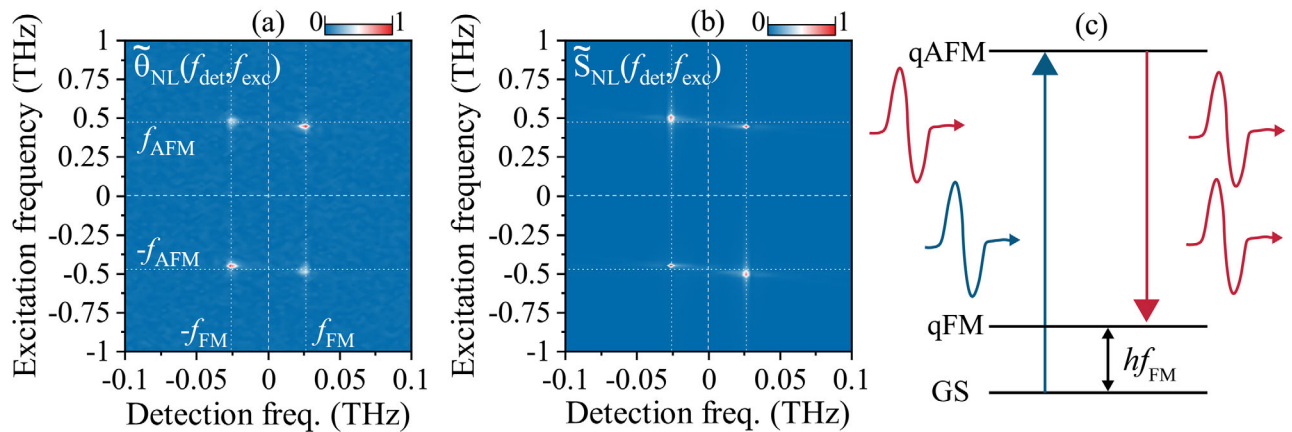


FIG. 4. (a) 2D FFT of the nonlinear part of the experimental data. The off-diagonal peaks indicate a nonlinear transfer of energy from the qAFM mode to the qFM mode, supporting the result of Fig. 3. (b) The 2D FFT of the nonlinear part of the simulated data  $S(t, \tau) = l_y(t, \tau) + l_z(t, \tau)$ . (c) Energy diagram of magnonic stimulated Raman scattering (MSRS). Here, the first THz pulse excites the qAFM magnon and the second THz pulse stimulates the Stokes transition to the qFM magnon state. Analogously, this effect induced by a single THz pulse [23] can be regarded as impulsive MSRS.

Considering that the input data  $\theta_{\text{NL}}$  are real, the 2D FFT is inversion symmetric  $\tilde{\theta}_{\text{NL}}(-f_{\text{det}}, -f_{\text{ex}}) = \tilde{\theta}_{\text{NL}}(f_{\text{det}}, f_{\text{ex}})$  such that we only need to consider positive  $f_{\text{det}} \geq 0$ . Note that due to peculiarities of 2D THz spectroscopy, the “rephasing” signals in the lower quadrant with  $f_{\text{ex}} < 0$  and “nonrephasing” signals in the upper quadrant with  $f_{\text{ex}} > 0$  (see Ref. [15]) are slightly shifted in the excitation frequency  $|f_{\text{ex}}| = |f_{\text{AFM}} \pm f_{\text{FM}}|$ , respectively. This shift is explained in detail in the Supplemental Material [25] and can be attributed to an effect similar to the Doppler effect. In general, the result of Fig. 4(a) implies energy transfer between the modes [13], and again reveals that the nonlinear excitation of the low-frequency qFM mode is modulated by the seemingly orthogonal qAFM mode.

To formally describe the discovered nonlinear coupling, we employ the Lagrangian formulation of the sigma model (see Refs. [6–8] and Supplemental Material [25]). Usually, this Lagrangian  $\mathcal{L}$  is only treated in linear approximation, in which case it can be divided into two mutually independent parts  $\mathcal{L} \approx \mathcal{L}_{y,0} + \mathcal{L}_{z,0}$ :

$$\begin{aligned} \frac{2\gamma H_{\text{ex}}}{\hbar} \mathcal{L}_{y,0} &= \left( \frac{\partial l_y}{\partial t} \right)^2 - \omega_{\text{FM}}^2 l_y^2 + 2\gamma^2 H_{\text{eff}} l_y h_x, \\ \frac{2\gamma H_{\text{ex}}}{\hbar} \mathcal{L}_{z,0} &= \left( \frac{\partial l_z}{\partial t} \right)^2 - \omega_{\text{AFM}}^2 l_z^2 - 2\gamma l_z \frac{dh_y}{dt}. \end{aligned} \quad (2)$$

Here  $H_{\text{eff}} = H_0 + H_{\text{D}}$  with  $H_{\text{D}}$  the Dzyaloshinskii-Moriya interaction field,  $\hbar$  is Planck’s constant, and  $\omega_{\text{FM}}$  and  $\omega_{\text{AFM}}$  are the angular frequencies of the magnetic modes. The first term  $\mathcal{L}_{y,0}$  describes the dynamics of the  $y$  projection of normalized Néel vector  $\mathbf{I} = \mathbf{L}/|\mathbf{L}|$  and thus corresponds to the qFM mode, while  $\mathcal{L}_{z,0}$  describes dynamics of the  $z$  projection that can be assigned to the qAFM mode [see Fig. 2(b)]. The equations of motion derived from these Lagrangians are not coupled and possess a substantial difference regarding the THz excitation. The dynamics of the  $z$  component  $l_z(t)$ , i.e., the qAFM mode, can be triggered efficiently by the THz magnetic field when this field is aligned perpendicular to the spins  $\mathbf{h} \perp \mathbf{L}$  [24]. The amplitude of the resulting oscillations in  $l_z(t)$  will be a linear function of the THz magnetic field. In principle, this linear mechanism can also excite the qFM mode when the THz magnetic field is aligned perpendicular to the weak magnetization  $\mathbf{M}$ . However, such a linear excitation is expected to be inefficient due to the absence of a strong spectral component at the qFM resonance frequency in the THz excitation spectrum; hence, it was not observed [23].

Thus, to explain the excitation of the qFM mode via coupling to the qAFM mode, we need to go beyond the linear approximation. Therefore, we included the nonlinear coupling term of the lowest order:

$$\frac{H_{\text{ex}}}{\hbar} \mathcal{L}_{\text{coupl}} = h_x \left( l_z \frac{dl_y}{dt} - l_y \frac{dl_z}{dt} \right). \quad (3)$$

This term results in a driving force  $\propto h_x(dl_z/dt)$  for the qFM mode coordinate  $l_y(t)$ . The oscillating part  $(dl_z/dt)$  launched by the first THz pulse modulates the excitation of the qFM mode as a function of the timing of the second THz pulse  $\tau$  at the frequency  $f_{\text{AFM}}$ . This modulation is confirmed analytically in the Supplemental Material [25]. The fact that the qAFM mode is excited linearly  $l_z(t) \propto h_y$  implies that the nonlinear excitation  $h_x(dl_z/dt) \propto h_x h_y$  scales quadratically with the THz field amplitude and occurs without threshold. The effect depends on the THz pulse shape and spectrum, as the THz pump spectral components at the qAFM frequency  $f_{\text{AFM}}$  and the difference frequency  $f_{\text{AFM}} - f_{\text{FM}}$  determine the strength of the excitation mechanism.

To demonstrate that the nonlinear coupling term of Eq. (3) explains the data, we derived the corresponding equations of motion for  $l_y(t)$  and  $l_z(t)$  and numerically solved the magnetization dynamics triggered by two pulses of THz magnetic field  $\mathbf{h}(t, \tau) = \mathbf{h}_1(t) + \mathbf{h}_2(t, \tau)$  (see Supplemental Material [25] for more details). Figure 4(b) shows the 2D FFT of the nonlinear part of the simulated signal  $S(t, \tau) = l_y(t, \tau) + l_z(t, \tau)$ . Note that experimentally we detected a projection of  $\mathbf{M}(t, \tau)$  that equals some linear combination of  $l_y$  and  $l_z$ . However, the current choice of  $S$  already exposes the nonlinear magnon-magnon coupling, and Fig. 4(b) has a good qualitative agreement with the experiment. This result allows us to conclude that this nonlinear term adequately describes the observed coupling between otherwise noninteracting modes of spin precession in FeBO<sub>3</sub>.

Using this theory, we could analytically estimate how much the susceptibility of the qFM mode to a THz magnetic field pulse is enhanced by the qAFM mode. We expressed this enhancement by the amplification factor  $\mu$  defined as the ratio of excitation efficiency of the qFM mode by the excitation pulse with and without the preparation pulse present (see Supplemental Material [25]). In the case of FeBO<sub>3</sub>, having a relatively large spin canting in the ground state, and for moderate THz magnetic fields  $|\mathbf{h}_{1,2}| \sim 0.1$  T, the amplification factor is estimated to be  $\mu \sim 7$ . Simple estimates show that when applying higher but realistic THz magnetic fields  $> 0.3$  T [26,34] to antiferromagnets with a smaller spin canting, the enhancement can reach multiple orders of magnitude. As the employed model is very general, one can boost the susceptibility of spins in absolutely any antiferromagnet, with and without spin canting, by a nonequilibrium coherent magnonic state. The generality of the effect is highlighted by recent reports of similar magnon-magnon interactions in the canted antiferromagnets ErFeO<sub>3</sub> [35] and YFeO<sub>3</sub> [36].

To conclude, our results show that a coherent magnonic state can substantially change the properties of an antiferromagnet, enabling a new nonlinear path of controlling spins by a pair of THz pulses. This has been demonstrated

by showing that a coherent qAFM magnonic state in FeBO<sub>3</sub> mediates the excitation of the qFM mode by THz magnetic field. The effect is analogous to electronic or ionic Raman scattering [37,38], but involves exclusively magnonic excitations and can be thus called magnonic Raman scattering or THz-mediated magnon-magnon coupling, as illustrated in Fig. 4(c). Our work shows that although the efficient control of antiferromagnetism in thermodynamic equilibrium is still a challenge, the problem can be solved by pushing antiferromagnets into a non-equilibrium state where the susceptibility of spins to an external magnetic field is boosted. By combining various magnonic [35,36], phononic [38–40], and electronic excitations [41], one can generate and explore diverse non-equilibrium states and find which excitation (or a combination thereof) facilitates the fastest and the most energy-efficient control of antiferromagnetism.

The authors thank S. Semin and C. Berkhout for their technical support. The work was supported by de Nederlandse Organisatie voor Wetenschappelijk Onderzoek (NWO) and the European Research Council ERC Grant Agreement No. 101054664 273 (SPARTACUS). The contribution of E. A. M. has been funded by the Deutsche Forschungsgemeinschaft (DFG, German Research Foundation) Project No. 277146847–CRC 1238.

\*Corresponding author: t.blank@science.ru.nl

- [1] P. Němec, M. Fiebig, T. Kampfrath, and A. V. Kimel, Antiferromagnetic opto-spintronics, *Nat. Phys.* **14**, 229 (2018).
- [2] C. Song, Y. You, X. Chen, X. Zhou, Y. Wang, and F. Pan, How to manipulate magnetic states of antiferromagnets, *Nanotechnology* **29**, 112001 (2018).
- [3] T. Jungwirth, X. Marti, P. Wadley, and J. Wunderlich, Antiferromagnetic spintronics, *Nat. Nanotechnol.* **11**, 231 (2016).
- [4] V. Baltz, A. Manchon, M. Tsoi, T. Moriyama, T. Ono, and Y. Tserkovnyak, Antiferromagnetic spintronics, *Rev. Mod. Phys.* **90**, 015005 (2018).
- [5] T. Kampfrath, A. Sell, G. Klatt, A. Pashkin, S. Mährlein, T. Dekorsy, M. Wolf, M. Fiebig, A. Leitenstorfer, and R. Huber, Coherent terahertz control of antiferromagnetic spin waves, *Nat. Photonics* **5**, 31 (2011).
- [6] A. K. Zvezdin, Dynamics of domain walls in weak ferromagnets, *JETP Lett.* **29**, 553 (1979).
- [7] A. F. Andreev and V. I. Marchenko, Symmetry and the macroscopic dynamics of magnetic materials, *Sov. Phys. Usp.* **23**, 21 (1980).
- [8] E. G. Galkina and B. A. Ivanov, Dynamic solitons in antiferromagnets (review article), *Low Temp. Phys.* **44**, 618 (2018).
- [9] W. Kuehn, K. Reimann, M. Woerner, T. Elsaesser, R. Hey, and U. Schade, Strong Correlation of Electronic and Lattice Excitations in GaAs/AlGaAs Semiconductor Quantum Wells Revealed by Two-Dimensional Terahertz Spectroscopy, *Phys. Rev. Lett.* **107**, 067401 (2011).
- [10] M. Woerner, W. Kuehn, P. Bowlan, K. Reimann, and T. Elsaesser, Ultrafast two-dimensional terahertz spectroscopy of elementary excitations in solids, *New J. Phys.* **15**, 025039 (2013).
- [11] J. Lu, X. Li, Y. Zhang, H. Y. Hwang, B. K. Ofori-Okai, and K. A. Nelson, Two-dimensional spectroscopy at terahertz frequencies, *Topics Curr. Chem.* **376**, 6 (2018).
- [12] C. L. Johnson, B. E. Knighton, and J. A. Johnson, Distinguishing Nonlinear Terahertz Excitation Pathways with Two-Dimensional Spectroscopy, *Phys. Rev. Lett.* **122**, 073901 (2019).
- [13] E. A. Mashkovich, K. A. Grishunin, R. M. Dubrovin, A. K. Zvezdin, R. V. Pisarev, and A. V. Kimel, Terahertz light-driven coupling of antiferromagnetic spins to lattice, *Science* **374**, 1608 (2021).
- [14] T. G. H. Blank, K. A. Grishunin, K. A. Zvezdin, N. T. Hai, J. C. Wu, S.-H. Su, J.-C. A. Huang, A. K. Zvezdin, and A. V. Kimel, Two-Dimensional THz Spectroscopy of Nonlinear Phononics in the Topological Insulator MnBi<sub>2</sub>Te<sub>4</sub>, *Phys. Rev. Lett.* **131**, 026902 (2023).
- [15] J. Lu, X. Li, H. Y. Hwang, B. K. Ofori-Okai, T. Kurihara, T. Suemoto, and K. A. Nelson, Coherent Two-Dimensional Terahertz Magnetic Resonance Spectroscopy of Collective Spin Waves, *Phys. Rev. Lett.* **118**, 207204 (2017).
- [16] A. J. Kurtzig, R. Wolfe, R. C. LeCraw, and J. W. Nielsen, Magneto-optical properties of a green room-temperature ferromagnet: FeBO<sub>3</sub>, *Appl. Phys. Lett.* **14**, 350 (1969).
- [17] V. E. Dmitrienko, E. N. Ovchinnikova, S. P. Collins, G. Nisbet, G. Beutier, Y. O. Kvashnin, V. V. Mazurenko, A. I. Lichtenstein, and M. I. Katsnelson, Measuring the Dzyaloshinskii-Moriya interaction in a weak ferromagnet, *Nat. Phys.* **10**, 202 (2014).
- [18] L. V. Velikov, A. S. Prokhorov, E. G. Rudashevskii, and V. N. Seleznev, Antiferromagnetic resonance in FeBO<sub>3</sub>, *Zh. Eksp. Teor. Fiz.* **66**, 1847 (1974) [*Sov. Phys. JETP* **39**, 909 (1974)].
- [19] J. Schober, Precession modes and resonance absorption in the canted antiferromagnet FeBO<sub>3</sub>, *IEEE Trans. Magn.* **12**, 401 (1976).
- [20] R. Wolfe, A. J. Kurtzig, and R. C. LeCraw, Room-temperature ferromagnetic materials transparent in the visible, *J. Appl. Phys.* **41**, 1218 (1970).
- [21] A. V. Kimel, R. V. Pisarev, J. Hohlfeld, and T. Rasing, Ultrafast Quenching of the Antiferromagnetic Order in FeBO<sub>3</sub>: Direct Optical Probing of the Phonon-Magnon Coupling, *Phys. Rev. Lett.* **89**, 287401 (2002).
- [22] A. M. Kalashnikova, A. V. Kimel, R. V. Pisarev, V. N. Gridnev, A. Kirilyuk, and T. Rasing, Impulsive Generation of Coherent Magnons by Linearly Polarized Light in the Easy-Plane Antiferromagnet FeBO<sub>3</sub>, *Phys. Rev. Lett.* **99**, 167205 (2007).
- [23] E. A. Mashkovich, K. A. Grishunin, R. V. Mikhaylovskiy, A. K. Zvezdin, R. V. Pisarev, M. B. Strugatsky, P. C. M. Christianen, T. Rasing, and A. V. Kimel, Terahertz Optomagnetism: Nonlinear THz Excitation of GHz Spin Waves in Antiferromagnetic FeBO<sub>3</sub>, *Phys. Rev. Lett.* **123**, 157202 (2019).
- [24] K. Grishunin, E. A. Mashkovich, A. V. Kimel, A. M. Balbashov, and A. K. Zvezdin, Excitation and detection

- of terahertz coherent spin waves in antiferromagnetic  $\alpha$ -Fe<sub>2</sub>O<sub>3</sub>, *Phys. Rev. B* **104**, 024419 (2021).
- [25] See Supplemental Material at <http://link.aps.org/supplemental/10.1103/PhysRevLett.131.096701> for details on the calibration of THz pulses in GaP, details of 2D spectroscopy, the full analytical treatment of the sigma model, the explanation of the Doppler-like shift seen in the 2D FFT diagrams, and for all supplemental experimental and numerical results, which includes Refs. [8,13,23,26–32].
- [26] H. Hirori, A. Doi, F. Blanchard, and K. Tanaka, Single-cycle terahertz pulses with amplitudes exceeding 1 MV/cm generated by optical rectification in LiNbO<sub>3</sub>, *Appl. Phys. Lett.* **98**, 091106 (2011).
- [27] J. Hebling, G. Almási, I. Z. Kozma, and J. Kuhl, Velocity matching by pulse front tilting for large-area THz-pulse generation, *Opt. Express* **10**, 1161 (2002).
- [28] B. A. Ivanov, Spin dynamics of antiferromagnets under action of femtosecond laser pulses (review article), *Low Temp. Phys.* **40**, 91 (2014).
- [29] E. Rudashevsky, V. Seleznyov, and L. Velikov, Antiferromagnetic resonance in an ordered state induced by external magnetic field in FeBO<sub>3</sub> over the Néel temperature, *Solid State Commun.* **11**, 959 (1972).
- [30] A. V. Kimel, B. A. Ivanov, R. V. Pisarev, P. A. Usachev, A. Kirilyuk, and T. Rasing, Inertia-driven spin switching in antiferromagnets, *Nat. Phys.* **5**, 727 (2009).
- [31] A. Y. Galkin and B. A. Ivanov, Dynamics of antiferromagnets exposed to ultrashort magnetic field pulses, *JETP Lett.* **88**, 249 (2008).
- [32] L. Landau and E. Lifshitz, *Course of Theoretical Physics: Vol. 1: Mechanics* (Reed Educational and Professional Publishing Ltd., Oxford, 1976).
- [33] I. Noda, Two-dimensional infrared spectroscopy, *J. Am. Chem. Soc.* **111**, 8116 (1989).
- [34] R. Rouzegar, A. L. Chekhov, Y. Behovits, B. R. Serrano, M. A. Syskaki, C. H. Lambert, D. Engel, U. Martens, M. Münzenberg, M. Wolf, G. Jakob, M. Kläui, T. S. Seifert, and T. Kampfrath, Broadband Spintronic Terahertz Source with Peak Electric Fields Exceeding 1.5 MV/cm, *Phys. Rev. Appl.* **19**, 034018 (2023).
- [35] Z. Zhang, F. Y. Gao, Y.-C. Chien, Z.-J. Liu, J. B. Curtis, E. R. Sung, X. Ma, W. Ren, S. Cao, P. Narang, A. von Hoegen, E. Baldini, and K. A. Nelson, Terahertz field-driven magnon upconversion in an antiferromagnet, [arXiv:2207.07103](https://arxiv.org/abs/2207.07103).
- [36] Z. Zhang, F. Y. Gao, J. B. Curtis, Z.-J. Liu, Y.-C. Chien, A. von Hoegen, T. Kurihara, T. Suemoto, P. Narang, E. Baldini *et al.*, Three-wave mixing of anharmonically coupled magnons, [arXiv:2301.12555](https://arxiv.org/abs/2301.12555).
- [37] M. Först, C. Manzoni, S. Kaiser, Y. Tomioka, Y. Tokura, R. Merlin, and A. Cavalleri, Nonlinear phononics as an ultrafast route to lattice control, *Nat. Phys.* **7**, 854 (2011).
- [38] D. M. Juraschek, D. S. Wang, and P. Narang, Sum-frequency excitation of coherent magnons, *Phys. Rev. B* **103**, 094407 (2021).
- [39] A. S. Disa, M. Fechner, T. F. Nova, B. Liu, M. Först, D. Prabhakaran, P. G. Radaelli, and A. Cavalleri, Polarizing an antiferromagnet by optical engineering of the crystal field, *Nat. Phys.* **16**, 937 (2020).
- [40] D. Afanasiev, J. R. Hortensius, B. A. Ivanov, A. Sasani, E. Bousquet, Y. M. Blanter, R. V. Mikhaylovskiy, A. V. Kimel, and A. D. Caviglia, Ultrafast control of magnetic interactions via light-driven phonons, *Nat. Mater.* **20**, 607 (2021).
- [41] S. Baierl, M. Hohenleutner, T. Kampfrath, A. K. Zvezdin, A. V. Kimel, R. Huber, and R. V. Mikhaylovskiy, Nonlinear spin control by terahertz-driven anisotropy fields, *Nat. Photonics* **10**, 715 (2016).